Tracking Storm-Generated Waves in the Northeast Pacific Ocean with ERS - 1 Synthetic Aperture Radar Imagery and Buoys

Benjamin Holt
Jet Propulsion Laboratory
California Institute of Technology

Antony K. Liu
NASA/Goddard Space Flight Center

H. S. Chen
NOAA/National Weather Service

Anand Gnandesikan
Geophysical Fluid Dynamics Laboratory

David W. Wang
Computer Sciences Corporation

Submitted to Journal Geophysical Research Oceans

February 3, 1997

Abstract

This paper examines the capability of synthetic aperture radar imagery from ERS- 1 and buoys to track the wave field emanating from an intense storm over a several day period. The first part of the study is a validation component that compares SAR-derived wave length and direction with buoy data from two locations from 10 different dates in late 1991. When the SAR is linear (8 out of 10 cases), mean wave length is within 5% of the buoy measurements and mean wave direction within 10 of direction derived from a wave model (albeit with large standard deviation of 270), indicating close agreement. The wave field generated from the intense storm in late December 1991 was measured by three separate ERS - 1 SAR passes across a 3-day period. A simple kinematic model was used for waves propagating from a storm. Comparing the model results with both SAR and buoy data indicate that SAR-derived wave length and direction measurements estimates can be reliably used to predict arrival times and propagation direction over a several day period and considerable distances. The measurements can also be used to derive estimated wave generation source regions about the storm as well. Such measurements are useful for comparing with wave model results, which perform less accurately for direction than wave height for example, and for predicting hazardous conditions for ship navigation and coastal regions.

I. Introduction

The tracking of storms and their associated wave fields is of interest both scientifically, for understanding wind-wave generation physics and its inclusion into wave models, and operationally for monitoring potentially hazardous conditions for shipping routes and coastal environments. Early studies showed that swell could be accurately identified as emanating from storms thousands of kilometers away (Barber and Ursell,1948; Munk et al., 1963; Snodgrass et al., 1966). Current global third generation wave models (WAM) attempt to forecast wave conditions based on integrated wind fields assimilated from satellite imagery and atmospheric soundings, and much improved wind and wave physics (WAMDI Group, 1988; Komen et al., 1994). While considerable improvements have been made in predicting wave height from severe storms and rapidly rotating winds since the SWAMP Report (1985), some problems still exist in predicting the directional wave energy distribution. Some of these problems are due to the model resolution of propagation direction (generally 30 degrees) which will improve with increased computer capabilities. Others are due to difficulties in determining the source regions of high storms, found to be located in the lower right quadrant of a moving storm. Waves generated from severe storms approaching landfall clearly can lead to potentially dangerous conditions for coastal inhabitants and directional accuracy is of prime importance (Wang and Carolan, 1991; Earle et al., 1984). Established networks of wave buoys, usually relatively close to shore, can provide valuable and near-real time data on wave fields, but generally do not provide wave directional information. The use of satellite imagery especially from synthetic aperture radar (SAR) can generally improve directional information and prediction accuracy (Beal, 1991; Komen et al., 1994).

Satellite imagery from synthetic aperture radar (SAR) provides a unique two-dimensional, fine-resolution (usually 25 m) view of the ocean surface, especially waves. From this view, wave length, propagation direction, and height information can be derived. One of the key applications of SAR has been in providing valuable information on the properties of storm-generated ocean waves. When the SAR is operating linearly over the ocean, it has been shown to provide accurate measurements on the evolution of wave fields (Beal et al., 1986; Beal, 199 1), the spatial properties of hurricane-generated waves (McLeish and Ross, 1983; Holt and Gonzalez, 1986; Monaldo et al., 1993), the improvement in wave information surrounding storms compared to wave models (Beal, 1991; Monaldo and Beal, 1996), and the source regions of storm-generated waves (Gonzalez et al., 1987). However the key word here is 'linear', which occurs primarily when the SAR is detecting swell or when the radar platform has a low shuttle-like orbital altitude (200-400 km). The problem is that SAR imagery of ocean waves and

derived SAR wave spectra can be severely nonlinear, due to the simple fact that the waves are moving at the same time the radar is precisely measuring the Doppler frequency of the moving SAR platform.

The non-linear conditions occur primarily when waves are traveling in a direction parallel (or in azimuth-traveling) to the platform flight direction. This simultaneous wave-platform motion can result in a distorted mapping of waves to imagery because the precisely timed radar returns from the waves have slightly varying Doppler frequencies and rates, termed velocity bunching. The result is either a shifting of the wave energy or actual non-imaging of wind waves moving in the azimuth direction. In addition, the SAR resolution may be degraded by coherence time limitation of the moving smaller waves (Raney, 1980). Both conditions are alleviated by decreasing the ratio of the platform range-to-target compared to platform velocity. Many researchers have long sought to understand the non-linearities sufficiently in order to correct for these by applying transfer functions (e.g. Hasselmann et al, 1985; Plant, 1992; Krogstad, 1992). Understanding has progressed sufficiently to the point that SAR image spectra from the European Space Agency's ERS systems are being used reliably, albeit at considerable computational cost, in SAR wave data assimilation schemes for global wind and wave model forecasts (Hasselmann and Hasselmann, 199 1; Engen et al., 1994; Komen et al., 1994).

This study examines the capability of spaceborne synthetic aperture radar (SAR) imagery, obtained from ERS-1, and buoy data to track a wave field generated by an intense storm in the northeast Pacific over a several day period. The SAR imagery and wave spectra were obtained from the ERS - 1 geophysical product system at the Alaska SAR Facility (ASF) during September - December 1991. First we establish the accuracy of the SAR spectra, which was accomplished by comparing 10 separate examples of SAR data nearly coincident in time and location to two sets of buoy data, one set operated by the National Data Buoy Center (NDBC) and another set deployed during a field experiment off Vancouver Island run by Woods Hole Oceanographic Institute (Galbraith et al., 1994). The validation segment determined that the SAR spectra were largely linear, which is related to the mean climatological conditions of the northern Pacific and the orientation of the orbital track. From this, the tracking of the storm waves could proceed with some confidence. The results from the SAR wave spectra are compared with buoy data for waves generated during a storm in late December 1991. For the case study, we describe a wave kinematic model, the storm, and then track the wave field over a three day period.

II. Data Set Description

A. Radar Imagery

The ERS - 1 SAR imagery was acquired in the Gulf of Alaska along the general tracks outlined on Figure 1 from September-December 1991, during the 3-day repeat of the mission's Commissioning Phase. ERS-1 is in a sun-synchronous orbit of about 98° and has a flight direction (azimuth angle) of about 196°T over the Gulf of Alaska during descending passes. The SAR operates at a frequency of 5.3 GHz (C-band, 5 cm wave length) over a fixed range of incidence angles from 20-26°, which results in a swath width of 100 km. The resolution of the processed imagery is 25 meters in both range and azimuth directions and the data are formatted into 12.5 m pixels. The imagery was acquired, processed, and distributed by the ASF, which is located at the University of Alaska in Fairbanks.

The SAR wave spectra were generated from the fine resolution imagery using a wave product algorithm in the. ASF-Geophysical Processor System (ASF-GPS), which also generated ice motion and ice classification products (Stern et al., 1994). The wave algorithm has been previously tested using Seasat imagery (Wadhams and Holt, 1991). For each image (100 by 100 km), the wave product algorithm performs a 2-dimensional digital Fast Fourier Transform on 16 subscenes, each 6.4 km by 6.4 km in size, which are contiguous in the azimuth direction and centered along the median range line. The resulting unsmoothed spectral density estimate has a spectral resolution of $Ak = (1/256)\ 2\pi/25$ rad $m^{-1} = 0.001$ rad m^{-1} and a chi-square distribution with 2 degrees of freedom (Monaldo, 1991). To reduce sampling variability, each spectrum is smoothed using a moving Gaussian filter with a full width of21 by 21 pixels and a kernel size of 5 pixels. The smoothing increases the degrees of freedom to 164 on the basis of the effective area of the filter (Beal et al., 1986). A peak finding routine locates the dominant local maxima or wave peaks and determines the wave length and direction of the peaks by their distance and orientation from the spectra center. The wave spectra are displayed as contour plots, as seen in Figure 2A. Wave direction has a 180° ambiguity which is generally resolved by examining weather data. For this analysis, the mean and standard deviation of the wave length and direction of the dominant wave peaks for a single scene arc obtained from all 16 subscenes, which assumes that the wave field is approximately homogeneous over a 100 km image frame. No other corrections have been made to the SAR imagery for either system or modulation transfer functions. As further described in Wadhams and Holt (1991), based on analysis by Monaldo (1991) and the characteristics of the smoothing filter, the theoretical SAR wave spectral precision is $\pm 2°$ in wave direction and ± 0.002 rad m^{-1} in wavenumber.

B. NDBC Buoy Data

Wave data from three separate National Data Buoy Center (NDBC) moored buoys were utilized in this study (Figure 1). Buoys 46001 and 46003 are 6-m NOMAD (Navy Oceanographic and Meteorological Automatic Device) deep-ocean buoys in the Gulf of Alaska. Data used from these buoys include wave period, significant wave height (H_S), wind speed, wind direction, and barometric pressure. All of the NOAA data used in the validation portion of the study were derived from 46001, since it was closest in location to the SAR orbital tracks. A third buoy used is 46042, a 3-m coastal wave buoy which also provides wave direction. All wave data are averaged over 20 minute periods. The accuracies of the wave parameters are as follows: significant wave height, ±0.2 m or 5%; wave period, ±1s; wave direction, ±5%.

C. Field Experiment Buoy Data

During the late fall and early winter of 1991, an array of buoys was deployed off the coast of Vancouver (49.2°N, 131.9°W) as part of the 1991 Acoustic Surface Reverberation Experiment (ASREX 91) (Figure 1) (Galbraith et al., 1994). Two of the moorings were waverider buoys, the first a Wavescan from Seatex A/S of Norway and the other a Wavetrack from Endeco/YSI of Marion, MA. The Seatex buoy obtains 2048 data points at 1 Hz every 3 hours, while the Endeco buoys obtained 2048 points at 2 Hz every 12 hours. The Seatex operated from November 1 to December 4, 1991 and was used in the validation segment of this study, while the Endeco buoy operated through the end of December, 1991, providing data for the storm tracking segment of the study. Also included in the mooring array were a series of meteorological measurements. A time series of significant wave height and period derived from Seatex buoy measurements during its period of operation and corresponding wind direction is shown in Figure 3.

D. Wave model data

Wave hindcast (3-hour interval) data were also obtained from the National Meteorological Center using the WAM model (Chen, 1995; WAMDI Group, 1988), which provides estimates of wave direction along with the four other parameters also obtained from the NDBC deep water buoys. Wave direction from these hindcasts was used in five cases for SAR validation, supplementing the measurements from the non-directional buoy 46001. This third-generation wave model has been used for operational forecasting since 1995 after several year's of development and comparison studies with the NDBC buoy data. The NMC uses Cycle 4 of the WAM, which incorporates both wind velocity and wave age for wave generation source functions, and a quasi-linear theory of wind-wave generation (Janssen, 1989; Janssen, 1991). The model runs twice daily to predict global ocean wave spectra for both 12 hour hindcasts and

72-hour forecasts. The model has a grid of 2.5 degrees (latitude and longitude). The wave spectrum is represented by 25 logarithmically-spaced frequencies with the ratio of frequency increment to its frequency being equal to 0.1 and wave directionality in 30 degree bins.

III. Validation of SAR-Derived Wave Measurements

A. SAR-Buoy Comparisons

Before using the SAR wave spectra for the storm-tracking case study, an assessment of the measurement accuracy of the SAR-derived wave length and wave direction was performed using comparisons with NDBC buoy 46001 and the WHOI data sets over varying environmental conditions. Ten separate ERS- 1 SAR data sets were utilized, five for buoy 46001 and five for the ASREX Seatex buoy. Table 1 lists the dates and time of each SAR pass. The environmental conditions for each date are detailed in Appendix A. For the comparisons with buoy 46001, buoy wave direction was derived from the WAM4 hindcasts. The SAR wave spectra were obtained from the SAR image frames closest to the two buoy locations, Track 1 -Frame A for 46001 and generally Track 3-Frame B for Seatex (Figure 1). The distances between the buoys and the SAR frames were variable, especially for the ASREX buoys, where the closest distance was at best 135 km. The key wave parameters for the SAR and buoys are listed in Table 1. Buoy wave length is derived from peak wave period using the deep water wave dispersion relationship $\lambda = T^2 g/2\pi$.

Figure 2a shows a representative SAR wave spectrum collected on November 2, 1991, which has a dominant wave length of216 m and propagation direction from 274°T. The frequency spectra from buoy 46001 is shown in Figure 2B and the hindcast results of the NMC WAM are shown in Figure 2C. The buoy results show the dominate wave period of about 12.4s (0.08 1 Hz), corresponding to a wave length of 239 m, and the WAM results show a propagation direction from 280°T. For the dominant peak wave component, the SAR spectrum compares reasonably well with the buoy results, however the SAR spectral shape is slightly distorted in the azimuth direction by the radar transfer function as compared to the model results.

Referring back to Table 1, it can be seen that of the 10 cases, 8 comparisons between the SAR measurements and the buoy measurements are favorable, while 2 cases, October 15 and November 16, show considerable differences in wave length and direction. We believe these differences are due to non-linearities in the SAR spectra resulting from azimuthal distortion and so are not considered in the following error calculations (more discussion below). Figure 4 shows the comparison of the 8 linear SAR-derived wave lengths and buoy wave periods using

the dispersion relation. Here we see that the SAR-derived wave lengths follow the relation but are slightly underestimated.

For the eight cases, the mean fractional difference in wave length is -5.1% with a standard deviation of 9.6% and the mean difference is -22m with a standard deviation of 31 m. Using the wavenumber precision of 0.002 rad/m (Monaldo, 1991), over the approximate range of measured buoy wave lengths (100-600 m), the theoretical accuracy in the wave length measurements are between 3% -20%, respectively. This average compares well with the mean absolute difference of 9.6% (29.4 m), as does the spread of accuracies over the wave length spread, since the largest discrepancies between buoy and SAR are generally those cases with the longest wave lengths. For direction, the mean difference is -0.8° as compared with the theoretical error of* 2° (Monaldo, 1991), but there is a wide standard deviation of 27.5°. Much of the directional differences arise from the storm in late December discussed in the case study. From these two assessments, the mean errors in wave length and direction fall within the expected ranges when the SAR wave spectra are linear.

To assess the tendency of the SAR spectra to be linear or nonlinear in the case of the two unfavorable measurements, we use the relation referred to as the velocity bunching parameter C described in Alpers (1983). Significant non-linearities occur if $C > \pi/2$, indicating that shifts of spectral peaks toward lower wave numbers are likely to occur. More specifically, nonlinear mapping results from a surface scatterer having a velocity component radial to the SAR look direction. The resultant displacement of the scatterer on the SAR image is in the azimuth or along-track direction (in all cases, the spacecraft heading is about 195°T). Random shifts cause the image to be smeared in the azimuth direction, which causes a decrease in response for high azimuth wavenumbers in the image spectra. This relation takes into account the range of the spacecraft to the target over the platform velocity (WV), wave length, H_S, the peak wave propagation direction relative to the azimuth or flight direction, and the radar incidence angle. For ERS-1 the R/V ratio is about 115 s. As shown in Table 1, values of C near 2 or greater are obtained for the two nonlinear cases on October 15 and November 16, due to the comparatively short wave length and large Hs in both cases. The remaining 8 cases have values generally much less than 1.5. The one other case with azimuth-traveling waves, October 24, shows reasonable comparisons in direction and wave length or no obvious distortions in the wave spectra, despite a generally high C value.

B. Comparison with Other SAR Wave Validation Studies

During the early months of ERS - 1 in 1991, several validation campaigns took place to assess the capability of the SAR for generating useful wave information. The Grand Banks validation program, summarized in Dobson and Vachon (1994), had the following key results: ERS- 1 SAR accurately measured long wave length swell, the SAR did not measure any azimuth-traveling waves shorter than 200 m but range-traveling waves were measured as short as 50 m (Vachon et al., 1994). For the winter conditions seen in the Grand Banks area, a majority of the SAR acquisitions were obtained of azimuth-traveling waves. Quasi-linear remapping was more effective than non-linear remapping to invert the problematic SAR spectra (Krogstad et al., 1994). Lastly, SAR and wave models were found to be complementary, since SAR was best at mapping swell and the wave model was best at mapping wind seas. Similar results were found in other validation experiments (Kleijweg and Greidanus,1993; Tilley and Beal, 1994). These results were essentially as predicted, based on years of analysis using SAR imagery from satellite, shuttle, and airborne platforms. To make full use of the ERS- 1 SAR wave mode data, where small 5 km vignettes are sampled every 200 km on a global basis, a non-linear inversion algorithm has been developed, which the SAR spectra are remapped in an iterative fashion together with the wave model WAM (Hasselmann and Hasselmann, 1991). Results indicate that this is effective in producing accurate measurements of wave length, direction as well as height (Komen et al., 1994).

C. Validation Summary

This validation component showed that SAR wave spectra derived using a simple filter and no transfer functions were found to be reasonably accurate in measurements of wave length and direction. This was largely fortuitous due to the meteorological conditions found in the northeast Pacific at least during the months September through December, 1991, when west -to-east swell (or range-traveling relative to the ERS - 1 flight direction) were predominantly measured, and hence, accurately mapped onto the SAR wave spectra. This dominant weather pattern is attributed to the semi-permanent Aleutian Low which is particularly intense during these early winter months (Overland and Heister, 1980). One circumstance, on October 24, did accurately measure short, azimuth-traveling waves, presumably due to the low wave height. The two cases where comparisons with buoy data were poor, October 15 and November 16, were due to the presence of variable wind seas and the proximity of the buoy to the storm center, respectively. Another case, in late December, resulted in large differences in wave direction, likely due to difficulties in modeling directional data from large storms, as will be discussed in the next section. Thus, under favorable conditions, these products can be reliably used for further investigations in this general region.

IV. Case Study of Storm and Swell Evolution

In this section, we examine the evolution of swell across the northeastern Pacific generated by a storm using SAR, buoys, and a kinematic wave model. The data set was identified by the fortuitous combination of a strong low pressure system, suitable SAR coverage of the emanating wave field, and buoy data both from NDBC and ASREX. We use a simple kinematic model derived by Gonzalez at al. (1987) to compare with the various buoy wave measurement sources. The synoptic weather chart of the storm on December 28, 1991 at 00Z is shown in Figure 5 and a location map of the ERS- 1 SAR tracks and buoys is shown in Figure 1.

A. Kinematic Wave Model

Using SAR wave spectra of a hurricane-generated wave field obtained from a shuttle-based (and hence lower altitude) platform and a simple kinematic wave model, Gonzalez et al. (1987) have shown that swell generally obey the linear wave theory of propagation and do not seem to be affected by propagation through zones of steady wind. It is assumed that the waves originate from nearly a point source or a generation region sufficiently far away to be considered as nearly a point source. Swell (wavenumber k) generation is defined as that point when the deep water group velocity

$$C_g = (g\,k)^{1/2} \tag{1}$$

exceeds the local wind speed component in the wave direction, where g is the gravity constant. The wave then ceases to be forced by the wind and begins to propagate freely as swell. By assuming such a swell system consists of free waves and is unaffected by other processes, such as wave-wave interaction and wave-current interaction, the swell directions at distant locations can be checked with the linear wave propagation model.

The geometry of the idealized storm swell kinematic model is shown in Figure 6 with the position of S (ϕ, λ) being the center of the swell generation region and P and C observation points. The great-circle distances to an observation point is given by (Snyder, 1987) to be

$$\sin\left(\frac{s}{2}\right) = \left[\sin^2\left(\frac{\phi_s - \phi_p}{2}\right) + \cos\phi_s \cos\phi_p \sin^2\left(\frac{\lambda_s - \lambda_p}{2}\right)\right]^{1/2} \tag{2}$$

wheres is the radian measure of the great-circle distance. The wave propagation direction or azimuth angle B_p at an observation point is found by combining two angles. The first angle θ_p is the internal angle subtended by two great circles, one that extends through S and P and the

other that extends through P and C. The second angle θr is the azimuth angle from P to C (SAR path). Spherical geometry (Figure 6) then determines the following relationship:

$$\theta_p = \cos^{-1}\left(\frac{\cos l - \cos s \cos d}{\sin s \sin d}\right) \quad (3)$$

and

$$s = C_g (t_p - t_s) \quad (4a)$$

$$l = C_g (t_c - t_s) \quad (4b)$$

In these relationships, if the quantities of (ϕ ,λ), C_g, and t_s are assumed known, then equations 2-4 can be solved for the swell propagation direction B_p and arrival time t_i for locations P and C.

B. Wave Data Comparison

Storm description. According to the surface synoptic weather analysis (Mariners Weather Log, 1992), a low pressure system developed near Japan on December 25, 1991, and moved rapid] y eastward. By December 27, at 12Z, it was a 962 mb storm near the dateline. At 00Z on December 28, the intensive storm had matured to a center pressure of 954 mb and was moving northeastward (about 60°) to a position of about 46”N, 179°E (Figure 5). The storm had begun to weaken and its forward speed to decrease by 00Z on December 29. Using the general concept that a storm’s most intense wind and wave generation zone is the lower right quadrant with respect to the storm’s path, this would place the intense wave generation zone on the southeast side of the northeast-traveling storm. The center of this swell generation zone is initially estimated to be 45°N, 177”W on the southwest side of the center of the storm, some 300 km distance from the storm center (Figure 1). Since the swell generation zone and time can be shifted for various propagation directions within the storm’s southeast quadrant, the postulated zones and time can be fine-tuned through iteration.

SAR Data. Data from three ERS-1 SAR acquisitions along descending orbits were obtained December 29, 30, and 31, 1991. Six SAR wave spectra were processed, at positions selected to sample the spreading of the wave field as well as to be close to the buoys (Figure 1). The wave length and wave direction from these spectra are listed in Table 2 and representative spectra from December 29 are shown in Figure 7. In all cases, the wave lengths are greater than 300 m and the wave directions are eastward or range-traveling with respect to the satellite track.

No non-linear mapping is apparent in any of the spectra. The longest waves (565 m) are from the northernmost spectra on December 29. As the available SAR data progress to the east and move later in time, wave length decreases but wave direction maintains a general clockwise rotation from north to south. This is seen at position A on the three tracks (2400-2530-2660), indicating the rotational spread of the wind source. Position B on Tracks 1 and 2 have nearly the same wave direction (265° and 267°) while being 23 hours apart, indicating that the locations of these images are well aligned with the wave propagation direction.

Buoy Wave Data. For this study, NDBC buoys 46001,46003, and 46042 have been utilized, noting again that 46042 is a directional buoy. From the WHOI-ASREX program, data from the non-directional Endeco buoy was used, since the directional Seatex buoy had already been recovered, Table 2 lists the key buoy information.

For buoy 46001, the low frequency peak of 0.05 Hz reached a maximum density and wave height of more than 6 m on December 29 at 2200Z (Figure 8), very close in time and position to the nearest SAR wave spectra. The contour plots for buoys 46001 and 46003 (Figure 9) show clearly the arrival of the 0.05 Hz peak at 46003 to be about 11 hours earlier than at 46001 due to its closer proximity to the storm center. This peak persisted at each buoy for at least 6 hours after arrival (Figure 10). The Endeco buoy showed the arrival time of the wave peak at 12Z on December 30 and a significant decrease in period 12 hours later. At buoy 46042, the same low (0.05 Hz) wavenumber peak arrived on December 31 at 0600Z, persisting for some 12 hours with a direction from 300 °(Figure 11).

Data Comparisons. It is clear from the buoy and SAR results that the peak storm wave field was captured at all four buoys at successive times and at least at the northern image from E2376. The remaining SAR frames sampled the storm waves after the wave field maximum had already passed through, This is primarily due to the sampling rate of the satellite being less than fortuitous. The southerly image of E2376 had a shorter wave length (388 m) than might be expected since it was only about 400 km to the south of its companion wave field which measured over 550 m in wave length. The smaller measurement may be caused by a slightly less favorable generation direction which was not as parallel to the storm isobar contours. In terms of direction, the southerly end of E2390 and buoy 46042 had similar directional measurements for the peak wave field 9 hours apart.

C. Data-Model Results and Discussion

First we consider the arrival times measured by the group velocity derived from the SAR and buoy measurements (T_{C_g}), compared with the total elapsed time (AT) between the observations and the estimated storm source time (December 28, 00Z). It can be seen from Table 2 that by and large these measurements result in earlier arrival times, with the exception of the most distance buoy measurements (Endeco and 46042) where the derived arrival times are nearly equal to the elapsed times. The earlier times would indicate that the estimated source region needs updating by being moved further away, but the close times of the distance buoys suggest that the estimated source location and time is actually quite good.

The comparisons of direction estimated by the model results (B_p) with the SAR measurements are generally favorable. We see that the two southernmost measurements are nearly the same, while the remaining three northerly SAR measurements are 10° less (or rotated counterclockwise) from the model. The differences may be due to wave-current refraction as the wave field passes through the Alaskan Coastal Current. This small set of measurements does suggest that this simple kinematic model is adequate for describing the general fan-shaped directional wave information from a strong storm.

Next, we use the SAR directional measurements to iterate the storm wave generation zone. This can be done simply by adding the equivalent distance AS based on C_g for the difference in time between T_{C_g} and AT for each measurement (Table 3). Using Eq. 2, revised source regions are calculated for the 6 measurements, which results in an updated mean position of about 42°N,177°W, approximately 475 km from the storm center (46°N, 179°E) as compared to 300 km with the first estimated point source (45°N,177°W). Using the revised point source, we then recalculate T_{C_g} for the 4 buoys (Table 3), showing closer comparisons with AT. The revised source region is moved further back into the lower right quadrant with respect to storm travel (about 60”T). These results indicate that the peak waves were generated within a few hours of the original estimated time that the storm reached its lowest pressure. (December 28 at 00Z) and from a region some 300-500 km to the lower right of the storm with respect to its travel direction. This is compared to previous results from Gonzalez et al. (1987) showing waves being generated within 200-300 km of a hurricane center, a radius greater than expected from the generally 50-100 km of maximum hurricane winds. The larger radius for this Pacific storm is still contained within the tight isobars seen on Figure 5.

V. Summary

This study indicates that the wave length and direction from SAR measurements plus a simple kinematic model can be used to provide useful information on the wave field emanating from strong storms. Taken separately, the SAR spectra from either E2376 and E2390 can provide enough details to enable some predictive capability for determining the arrival time, energetic, and direction of large swell propagating from remote storms towards coastal areas. Samples from multiple SAR passes improves this predictive capability. The SAR directional information in particular can enhance both buoy data and wave models results as well as provide improved information on the wind fields from storms, including estimating the source region and generation time.

A key to using SAR for such studies and especially in an operational application is adequate sampling. Spaceborne SAR is either data-rate limited or power-limited, which prevent duty cycles (amount of time that the SAR can operate) greater than about 30%. The ERS SARS operate outside ground reception stations in its unique wave mode, producing 5 km vignettes every 200 km along-track. This is potentially a very useful mode except that the data are stored on-board and downlinked to a ground station when possible. This delay is at least 90-100 minutes or as much as several hours depending on how often the satellite comes into view per day of a ground station designated to receive such data. Also the spectral products from these vignettes are not yet operationally available. Spaceborne SARS have 14-16 orbits per day and limited swaths compared to operational sensors such as AVHRR. Options therefore for improving coverage arc to increase swath width (usually at the expense of resolution which is particularly important for wave imaging) such as with Canada's RADARSAT or to use multiple satellites placed in orbits 1-2 clays apart in their repeat pattern, such as ERS-1 and ERS-2 recently were in their Tandem Phase. Also of key importance is to get rapid data reception, processing, and incorporation of results with wave model and buoy data. The real-time SAR ocean wave spectra processor flown on two shuttle flights in 1994 demonstrated the capability of onboard processing from image data to wave spectra, which also significantly reduces data storage requirements (Monaldo and Beal, 1996).

This case study indicates the feasibility of using SAR in the advanced warning of high swell which could also be crucial to the safety of offshore operations and coastal regions. In general, the National Weather Service under predicts the storm surge along coastal areas. The water run-up of storm generated swell system in addition to the storm surge model will improve the storm surge prediction in the coastal zone. Such a system is feasible with current spaceborne

SARS for demonstration purposes at least and operationally in the future with improved ocean coverage and potentially onboard processing.

Acknowledgments

The authors wish to thank C. Y. Peng and Y. Y. Chao of GSFC for their valuable discussions and suggestions, Ron Kwok, Glenn Cunningham, Amy Rodgers, and Joanne Shimada of JPL for development of the ASF geophysical processing system and the ASF operational staff. The JPL effort was supported by the National Aeronautics and Space Administration through a contract with the Jet Propulsion Laboratory, California Institute of Technology. The GSFC work was supported by the National Aeronautics and Space Administration and Office of Naval Research.

Appendix. Environmental Conditions for Validation of ERS-1 SAR Data with Buoy Data

A brief summary is provided of the weather and wave environment for each of the ten dates used in the buoy/SAR validation (Table 1) based on NMC surface charts, site descriptions (Galbraith et al., 1994), and buoy and wave model results.

A. NDBC Buoy 46001

September 18. On September 17 and 18 a low pressure system to the west gradually moved northwestward and weakened later on September 18. Conditions were mild near the buoy until mid-day when a weak low pressure system south and east of the buoy. The buoy measured wind speeds near 10 m/s with a wind direction from about 270° at mid-day which gradually shifted to easterly during September 19 due to the front. H_s was near 3 m. The wave model indicated a wave direction from 230°. The SAR spectrum showed a very consistent peak at 179 m from around 250°, from the low pressure system to the west, and a less energetic peak of about 300 m from the north, with the later related to the closer system. This lower frequency peak was not seen on the buoy frequency spectra and may have been non-linearly mapped to a lower wavenumber on the SAR spectra, since it had a strong radial component nearly parallel to the flight direction.

October 15. No significant pressure systems were present near the buoy for the 15th. Winds had dropped slightly to 12 m/s from 15 m/s the day before. Modeled wave direction is 140°. The frequency spectra had a dominant period of 10 s and H_s of about 4 m. The dominant peak on the SAR spectra was at 157 m from a direction of 265°. A less energetic and quite variable peak in the SAR spectra is at 196 m from 134°, which aligns with the wind direction. The 157 m wave field may have emanated from a large low pressure system present far to the west. In summary, the lack of a significant pressure system has resulted in a variable wind sea on both the buoy and the SAR data, producing a somewhat confusing comparison. There appears to be non-linear mapping on the SAR spectra, even though the winds are some 40° off of the flight direction which would tend to reduce the azimuth component on the SAR spectrum.

October 24. A stable high pressure system south of Alaska resulted in a very mild period before and during the 24th. Wind speeds were less than 5 m/s and H_s was 1 m, and wind direction was from 180°. The wave model hindcast indicated a wave direction also of 180°. The dominant peak in the SAR spectra has similar measurements of 100 m from the south. In this case, then, short wave length azimuth-traveling waves were apparently accurately mapped on the SAR spectra, due primarily to the low Hs.

November 2. A low pressure system developed near the buoy during the 2nd, with two substantial low pressure systems to the west and south. Wind speeds were steady before and during this day at about 10 m/s from the west. The frequency spectra showed a stable 12 s wave field, also from the west according to the wave model (Figure 2). Hs was high at around 4.5 m. The SAR spectra showed a very steady 215 m wave field from nearly due west, comparing quite favorably with the buoy data.

December 29. The strong low pressure system discussed here is the same storm used in the case study discussed in section III. According to the surface synoptic weather analysis, a low pressure system developed near Japan on December 25, 1991, and moved rapidly eastward. By December 27, at 12Z, it was a 962 mb storm near the dateline. At OOZ on December 28, the intensive storm had matured with a center pressure of 954 mb, shifting northeastward (about 60°T) to a position of about 46°N,179°E (Figure 5). The storm had begun to weaken and its forward speed began to decrease by 00Z on December 29, finally passing very near buoy 46001 late on the 29th, with a pressure on 984 mb. The time series frequency spectra shows a peak with an increasing density coincident to the SAR data on 122921, indicating a peak of around 20s (Figure 8). The model wave direction is from 300°, although the wind direction is generally from the west. The SAR spectra is quite comparable at 565 m, with a direction slightly rotated southward of the wind direction.

B. AS REX Seatex buoy

November 4. A weak high pressure system passed by the mooring in the early part of the day, when the westerly winds dropped from 10 m/s to 3-4 m/s by about 08Z. Later in the day a weak low pressure system arose, which increased wind speeds to 9-10 m/s and shifted the wind direction to southerly. Wave heights remained constant at around 3-3.5 m, with the dominant low frequency peak emanating from a westerly direction of between (255-2700), having been generated from a strong low pressure system well to the west. These waves are orthogonal or range-traveling relative to the ERS- 1 flight direction of 196°. Thus these waves are not subject to nonlinear SAR mapping conditions and the buoy and SAR measurements are comparable.

November 16. A strong storm system passed over the mooring during the middle of this clay, reaching a low of about 968 mb near midday. This was followed at 18Z by peak winds of 22 m/s and H_S of 10 m with a maximum period of about 14-15 s. Earlier in the day, there was evidence of 3 wave systems; a low frequency system propagating from the west with about a 14 s period, a 12 s period from the south, and a wind sea from the southeast. With the storm, the wind sea and low frequency peaks steadily coalesced from a direction of about 240°. NMC

surface charts showed the center of the low at 49”N, 136°W at 12Z and 52°N, 133°W at OOZ on November 17, some 250 km to the west of the buoy.

As noted in Section II, the SAR data showed considerably different dominant wavefields. The location of the SAR data is slightly east of the estimated storm center, between the storm and the buoy. There was a 195 m wave field with a propagation direction from 288° and a 536 m wave component propagating from 175°. The westerly SAR wave field is shorter than that measured by the buoy earlier in the day and the southerly SAR wave field is considerably longer and rotated 60° towards the south from the dominant buoy component. Also the steep wind waves in the SAR region are undoubtedly mapped in a non-linear fashion on the imagery due to the strong wind component in the radial direction, nearly parallel to the flight direction, which resulted in a mapping to a lower wavenumber. The westerly wave component on the SAR imagery may be remaining from the earlier westerly component seen on the buoy data although it is much shorter in wave length. In conclusion, the strong rotating winds in the near-field to the SAR likely produced non-linear mapping of the wave field on the SAR spectra.

November 25.. At the time of the SAR overpass, the wind speeds had dropped to around 5 m/s from the south from a high of 12 m/s from the west late on November 24. Wave heights are relatively constant at around 2-3 m. The low frequency waves are propagating from the west. The SAR spectrum is broad from the west, but the dominant lobe is centered at 307°. Thus, under these relatively mild conditions, the measured wave lengths are quite comparable but the broad spectrum results in a less accurate angular measurement.

December 1. A high pressure system has remained in the area for several days. A high wind speed of 14 m/s occurred at 12Z from the northwest. Wave height remains around 3 m. The frequency spectra at the end of the day was unimodal at about 10 s with a directional peak at about 280°. The buoy and SAR comparisons are quite good.

December 4. A front passed over the mooring late on December 3, with wind directions shifting from southerly to westerly. During December 4 the winds shifted slowly back to the south, with the wind speeds remaining steadily at 10 rids. Wave height remains around 3-4 m. The low frequency swell is from the west, while the higher frequency waves track the wind. Again, the buoy and SAR comparisons of the dominant low frequency waves are good.

References

Alpers, W. R., Monte Carlo simulations for studying the relationship between ocean waves and synthetic aperture radar image spectra, J. Geophys. Res., 88(C3), 1745-1759, 1983.

Barber, N. F., and F. Ursell, The generation and propagation of ocean waves and swell, Phil. Trans. R. Sot. Lend., 240,527-560, 1948.

Beal, R. C., T. W. Gerling, D. E. Irvine, F. M. Monaldo, and D. G. Tilley, Spatial variations of ocean wave directional spectra, J. Geophys. Res., 91 (C2), 2433-2449, 1986.

Beal, R. C., editor, Directional Ocean Wave Spectra, Johns Hopkins University Press, Baltimore, 218pp., 1991.

Chen, H. S., Evaluation of a global ocean wave model at the National Meteorological Center, in Proceedings of the Second International Conference on Hydro-Science and -Engineering, March 22-26, 1995, Beijing, China, Tsinghua University Press, Beijing, 1436-1443, 1995.

Dobson, F. W., and P. W. Vachon, The Grand Banks ERS- 1 SAR wave spectra validation experiment, Atmosphere-Ocean, 32(1), 7-29, 1994.

Earle, M. D., K. A. Bush, and G. D. Hamilton, High-height long-period ocean waves generated by a severe storm in the Northeast Pacific Ocean during February 1983, J. Phys. Ocean., 14, 1286-1299, 1984.

Engen, G., H. Johnsen, H. E. Krogstad, and S. F. Barstow, Directional wave spectra by inversion of ERS - 1 synthetic aperture radar ocean imagery, IEEE Trans. Geosci. Remote Sens., GE-32, 340-352, 1994.

Galbraith, N. R., A. Gnanadesikan, G. H. Tupper, and B. S. Way, Meteorological and Oceanographic Data Collected during the ASREX 91 Field Experiment, Woods Hole Oceanographic Institution Tech. Rep. 94-1, Woods Hole, MA., 114 pp., 1994.

Gonzalez, F. I., B. Holt, and D. G. Tilley, The age and source of ocean swell observed in hurricane Josephine, Johns Hopkins Tech. Digest, 8,94-99, 1987.

Hasselmann, K., R. K. Raney, W. J. Plant, W. Alpers, R. A. Shuchman, D. R. Lyzenga, C. L. Rufenach, and M. J. Tucker, Theory of synthetic aperture radar ocean imaging: A MARSEN view, J. Geophys. Res., 90(C3), 4659-4686, 1985.

Hasselmann, K., and S. Hasselmann, On the nonlinear mapping of an ocean wave spectrum into a synthetic aperture radar image spectrum and its inversion, J. Geophys. Res., 96 (C6), 10,713-10,729, 1991,

Holt, B., and F. I. Gonzalez, SIR-B observations of dominant ocean waves near Hurricane Josephine, J. Geophys. Res., 91,8595-8598, 1986.

Janssen, P. A. E. M., Wave-induced theory of wind-wave generation applied to wave forecasting, J. Phys. Ocean., 19,745-754, 1989.

Janssen, P. A. E. M., Quasi-1 inear theory of wind-wave generation applied to wave forecasting, J. Phys. Ocean., 21, 1631-1642, 1991.

Kleijweg, J. C. M., and H. Greidanus, Validation of directional wave spectra from the ERS- 1 during the ESA Cal/Val campaign, Proceedings First ERS - 1 Symposium, Cannes, France, 4-6 November 1992, ESASP-359,31-34, 1993.

Komen, G. J., L. Cavalieri, M. Donelan, K. Hasselman, S. Hasselmann, and P. A. E. M. Janssen, Dynamics and Modeling of Ocean Waves, Cambridge University Press, 532 pp., 1994.

Krogstad, H. E., A simple derivation of Hasselmann's nonlinear ocean-SAR transformation, J. Geophys.Res.,C97,2421 -2425, 1992.

Krogstad, H. E., O. Samset, and I'. W. Vachon, Generalizations of the non-linear ocean-SAR transform and a simplified SAR inversion algorithm, Atmosphere-Ocean, 32(1), 61-82, 1994.

Mariners Weather Log, North Pacific Weather October, November, and December 1991,36 (2), 72-76.1992.

McLeish, W. M., and D. B. Ross, Imaging radar observations of directional properties of ocean waves, J. Geophys. Res., 88, 4407-4419, 1983,

Monaldo, F. M., The consequences of sampling variability on the estimation of wave number and propagation direction from spaceborne SAR image spectra, IEEE Trans. Geosci. Remote Sens., GE-29, 113-119, 1991.

Monaldo, F. M., T. G. Gerling, and D. G. Tilley, Comparison of SIR-B SAR wave image spectra with wave model predictions: Implications on the SAR modulation transfer function, IEEE Trans. Geosci. Remote Sens., GE-3 1, 1199-1209, 1993.

Monaldo, F. M., and R. C. Beal, Comparison of wave parameters measured from the SIR-C on-board processor with WAM predictions in the Southern Ocean, Johns Hopkins Report S lR-96-01, Laurel, MD, 37 pp., 1996.

Munk, W. H., G. R. Miller, F. E. Snodgrass and N. F. Barber, Directional recordings of swell from distant storms, Phil. Trans. R. Sot. Lend., 255,505-583, 1963.

Overland, J. E., and T. R. Heister, Development of a synoptic climatology for the northeast Gulf of Alaska, J. Applied Meteorology, 19, 1-14.1980.

Plant, W. J., Reconciliation of theories of synthetic aperture radar imagery of ocean waves, J. Geophys. Res., 97(C5), 7493-7501, 1992.

Raney, R. K., SAR response to partially coherent phenomena, IEEE Trans. Ant. Prop., AP-26, 777-787, 1980.

Snodgrass, F. E., G. W. Groves, K. F. Hasselmann, G. R. Miller, W. H. Munk, and W. H. Powers, Propagation of ocean swell across the Pacific, Phil. Trans. R. Sot.Lond.,431-497, 1966.

Snyder, J. P., Map projections-a working manual, U.S. Geological Survey Professional Paper 1395, U.S. GPO, 383 pp, 1987.

Stern, H. L., D. A. Rothrock, R. Kwok, and B. Holt, The geophysical processor system: automated analysis of ERS - 1 SAR imagery, Proceedings Second ERS - 1 Symposium, Hamburg, Germany, 11-14 October 1993, ESASP-361,281-286, 1994.

The SWAMP Group, Ocean Wave Modeling, Plenum Press, New York, 262 pp., 1985.

Tilley, D. G., and R. C. Beal, ERS-1 and Almaz estimates of directional wave spectra conditioned by simultaneous aircraft SAR and buoy measurements, Atmosphere-Ocean, 32(1), 113-142, 1994.

Vachon, P. W., H. E. Krogstad, and J. S. Paterson, Airborne and spaceborne synthetic aperture radar observations of ocean waves, Atmosphere-Ocean, 32(1), 83-112, 1994.

Wadhams, P., and B. Holt, Waves in frazil and pancake ice and their detection in Seasat synthetic aperture radar imagery, J. Geophys. Res., 96(C5), 8835-8852, 1991.

WAMDI Group, The WAM model-a third generation ocean wave prediction model, J. Phys. Oceanogr., 18, 1775-1810, 1988.

Wang, D. W.-C., and R. Carolan, Estimation of swell direction by a small discus buoy in high seas, in Proceedings of Fifth Conference on Meteorology and Oceanography of the Coastal Zone, May 6-9, 1991, American Meteorological Society, 53-59, 1991.

Tables

1, Comparison of SAR and buoy wave parameters

2. Storm tracking wave data

3. Revised storm tracking wave data

Figures

1. Map of the Northeast Pacific Ocean showing the location of buoys from NDBC (46003, 46001, and 46042) and ASREX, and representative SAR tracks for both the validation and storm tracking sections with darkened boxes indicating SAR spectra locations.

2. Comparison from November 2, 1991 at 2 lZof the (a) Alaska SAR Facility wave product spectrum from ERS- 1 SAR, and (b) buoy frequency spectra and c) WAM results for NDBC buoy 46001.

3. A time series from the ASREX Seatex buoy showing H_s, T_s, and wind direction from November 1 - December 5, 1991. The times of the five coincident SAR data are indicated by vertical dashed lines.

4. Comparison of measurements of wave period from buoy 46001 and wave length from ERS- 1 SAR using the wave dispersion relation. See Table 1 for details.

5. NMC surface analysis synoptic weather chart at OOZ on December 28, 1991. The low pressure region (954 mb) identifies the storm used in this study.

6. Geometry of the idealized storm swell kinematic model. The point S represents the source of swell generation, P and C are points of SAR imaging locations.

7. Alaska SAR Facility wave products of ERS - 1 SAR spectrum from December 29, 1991 (E2376) in the Northeast Pacific from (a) Track 1, frame **a,** and (b) Track 1, frame **b (see** Figure 1).

8. Time series of wave spectra from NDBC Buoy 46001 on December 29, 1991.

9. Contour plots of wave spectra from (a) Buoy 46001, and (b) Buoy 46003 during December 27-31, 1991.

10. Time series plot of peak wave spectral density for (a) Buoy 46001, and (b) Buoy 46003 during December 28-31, 1991.

11. Directional wave spectra from Buoy 46042 near Monterey, California at 042,062, 12Z, and 182 on December31, 1991.

Table 1. Comparison of SAR and buoy wave parameters

			SAR DATA			BUOY DATA						
BUOY	TIME	**DIST**	**SAR λ**	**SAR**	**DIR**	**C**	**T**	**λ**	**DIR**	**H_S**	**U**	**Δλ%**	**ΔDIR**
(Track-Pos)	MoDaHr k	m	m	deg			s	m	deg	m	m/s	m	deg
46001(la)	091821	58	179	252		1.09	11	189	230	3.0	8	-5	22
46001(la)	101521	38	157 196	265 134		2.28	IO	156	140	4.0	12	NL	NL
46001(la)	102421	38	103	I 95		1.39	8.3	107	180	1.0	4	-4	15
46001(la)	110221	25	216	274		0.21	12.4	239	280	4.5	8	-10	-6
46001 (la)	122921	25	565	240		0.22	20.0	624	300	6.0	14	-1o	-60
Seatex(3b)	110420	198	327	261		0.25	15.7	383	264	3.1	8	-15	-3
Seatex(3a)	111620	228	195 536	288 175		1.97	14.6	332	238	10	21	NL	NL
Seatex(3b)	112520	135	175	307		0.24	10.3	164	278	2.3	8	7	29
Seatex(3b)	120120	135	182	291		0.02	10.3	164	286	3.4	5	11	5
Seatex(3b)	120420	202	296	273		0.08	15.0	350	281	3.5	8	-15	-8
									—	—			
										Mean A		**-5.1**	-0.8
										Std **Dev**		9.6	27.5
									Mean Absolute A			9.6	18.5
									Std Dev			4.1	19.1

Table I Legend

Track - Pos = Track and position of SAR image. See Figure 1.
DIST = Distance from buoy to SAR image.
SAR λ = SAR-measured wave length of dominant peak.
SAR DIR= SAR-measured dominant peak wave direction from source.
C = Velocity bunching parameter. Reference is Alpers (1983).
T = Buoy wave period.
λ = Derived from T using dispersion relationship.
DIR = Wave direction from source, derived from WAM hindcast.
Hs = Significant wave height.
U = Wind speed
$\Delta\lambda$ = Fractional difference in wave length between buoy and SAR.
ADIR = Difference in wave direction between buoy and SAR.

Table 1 Notes

1). ERS-1 flight (azimuth) direction is 196°T for all images.
2) For Seatex direction, 21 degrees added for magnetic correction.
3). NDBC 46001 location= 56.3°N, 148.3°W.
4). WHOI ASREX Seatex location = 49. 15°N, 131.89°W.

Table 2. Storm Tracking Wave Data

SAR ORBIT (Track-Pos)/ BUOY	LOCATION Lat. Lon	TIME MoDaHr	DIST S k m	B_p deg	DIR deg	λ m	Hs m	C_g km/hr	T_{C_g} hr	A T hr
NDBC 46003	51.9, 155.9	1229:10	1723	---	---	624	7	**56.1**	**30.7**	**34**
NDBC 46001	56.3, 148.3	1229:22	2351	---	---	624	6	56.1	**41.9**	**44**
E2376 (la)	56.2, 149.8	1229:21	2260	250	240	565	---	53.4	**42.3**	**45**
E2376 (lb)	46.6, 153.3	1229:21	1835	264	265	388	---	44.0	**41.7**	**45**
Endeco	49.1, 131.8	1230:12	3395	---	---	624	4	56.1	**60.5**	**60**
E2390 (2a)	54.7, 142.0	1230:20	2698	263	253	373	---	43.4	**62.2**	**69**
E2390 (2b)	47.0, 144.8	1230:20	2479	278	267	316	---	40.0	**62.0**	**69**
E2390 (2c)	43.2, 145.9	1230:21	2476	286	288	317	---	40.5	**61.8**	**69**
Endeco	49.1, 131.8	1231:00	3395	---	---	433	6	46.8	**72.5**	**72**
NDBC 46042	36.8, 122.4	1231:06	4588	---	300	624	5	56.1	**81.8**	**82**
E2404 (3a)	53.5, 134.2	1231:20	3192	---	266	292	---	38.4	**83.1**	**92**

Table 2 Legend

SAR ORBIT (Track-Pos) = ERS - 1 (E) orbit number plus track and position of SAR image on Figure 1.

BUOY = Buoy identifier. Endeco buoy is located at ASREX site on Figure 1.

DIST S = Great circle distance from initial estimated storm wave generation region (45°N,177°W) to SAR image or buoy position using Eq.2.

B_p = Great circle angle of wave propagation direction using Eq. 3.

DIR = Direction from which waves are propagating measured from SAR or buoy spectra.

λ = Wave length measured directly from SAR spectra or derived from buoy-measured wave period using dispersion relation.

Hs = Significant wave height measured from buoy.

C_g = Group velocity derived from SAR or buoy measurement of wave length or period.

TC_g = Hours of wave travel time using C_g and DIST S.

AT= Time difference between estimated storm wave generation time (Dec. 28 00Z) and buoy or SAR wave length measurement.

Table 2 Notes

1) Bp for E2404 was not derived since there are only two of three points for Eq. 3.

Table 3. Revised Storm Tracking Wave Data

SAR ORBIT (Track-Pos)/ BUOY	DIST S km	DIR deg	C_g km/hr	T_{C_g}-Δ T A S hr	km	LAT LON deg N deg W/E	*TCg hr	AT hr
E2376 (la)	2260	240	53.4	1.7	91	42.4 174.8W		
E2376 (lb)	1835	265	44.0	3.3	145	42.3 177.7W		
E2390 (2a)	2698	253	43.4	6.8	273-295	40.8 176.6W		
E2390 (2b)	2479	267	40.0	7.0	260-280	40.5 178.0W		
E2390 (2c)	2476	288	40.5	7.1	271-288	45.7 179.4E		
E2404 (3a)	3192	266	38.4	8.9	342	41.4 179.7W		
NDBC 46003							34.4	34
NDBC 46001							46.2	44
Endeco [Time = 1230: 12]							63	60
NDBC 46042							82.8	82

Table 3 Legend

SAR ORBIT (Track-Pos) = ERS - 1 (E) orbit number plus track and position of SAR image on Figure 1.

BUOY = Buoy identifier. Endeco buoy is located at ASREX site on Figure 1.

DIST S = Great circle distance from initial estimated storm wave generation region (45°N,177°W) to SAR image or buoy position using Eq.2 (see Table 2).

B_p = Great circle angle of wave propagation direction using Eq. 3 (see Table 2).

DIR = Direction from which waves are propagating measured from SAR or buoy spectra (see Table 2).

C_g = Group velocity derived from SAR or buoy measurement of wave length or period (see Table 2).

(T_{C_g} - AT)= Travel time difference from Table 2.

AS = Change in km from $(TCg\text{-}\Delta T).C_g$.

LAT - LON = Revised storm wave generation source region based on DIR and AS.

*T_{C_g} = Revised hours of wave travel time using C_g, DIST S + AS, and mean of revised LAT-LON (42°N,177°W).

AT= Time difference between estimated storm wave generation time (Dec. 2800Z) and buoy or SAR wave length measurement (Table 2).

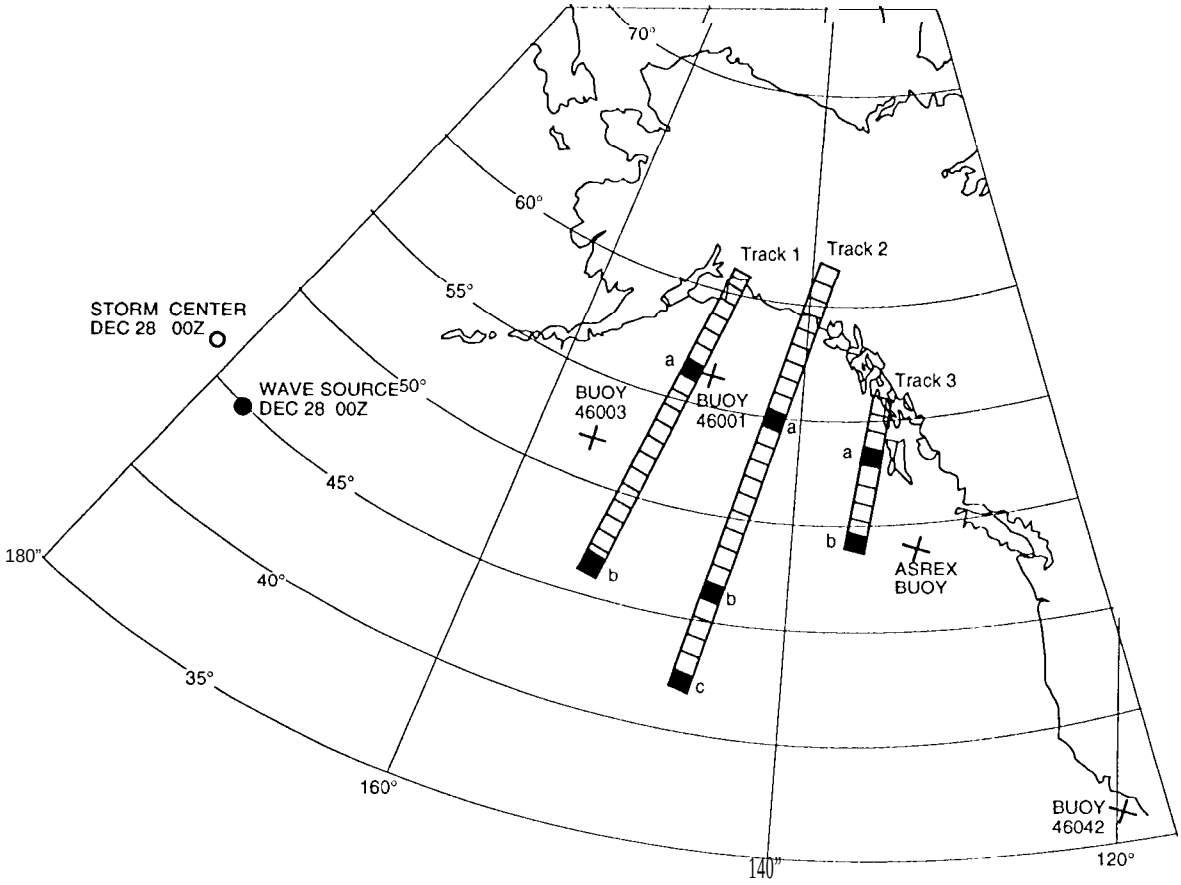
70°
60°
55°
50°
45°
40°
35°
180°
160°
140°
120°
STORM CENTER
DEC 28 00Z
WAVE SOURCE
DEC 28 00Z
Track 1
Track 2
Track 3
BUOY
46003
BUOY
46001
ASREX
BUOY
BUOY
46042
a
b
c

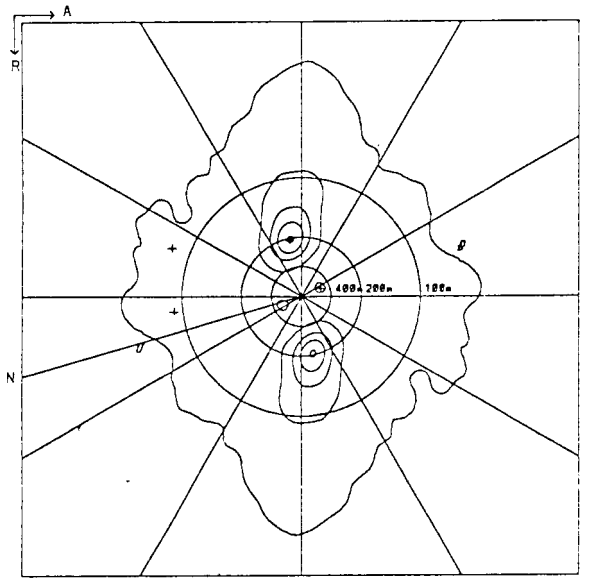

PEAK #	WAVE LEN (m)	DIR (deg wrt/N)	PEAK #	WAVE LEN (m)	DIR (deg wrt/N)
1	216.1	94.4, 274.4	4	96.3	2, 189.2
2	594.2	174.3, 354.3	5	73.6	17, 358.7
3	89.5	36.5, 216.5			

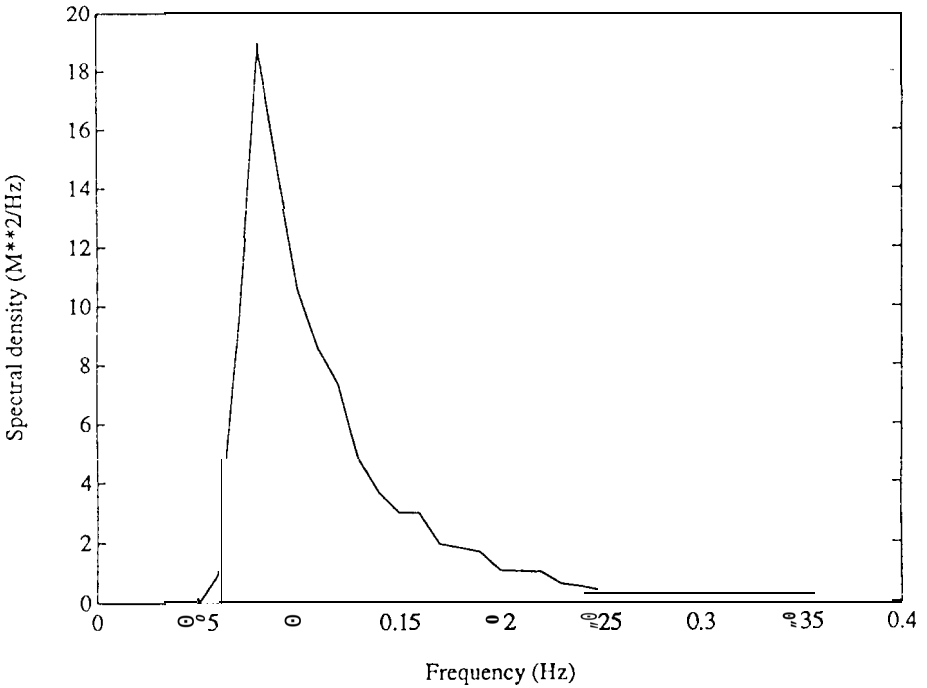

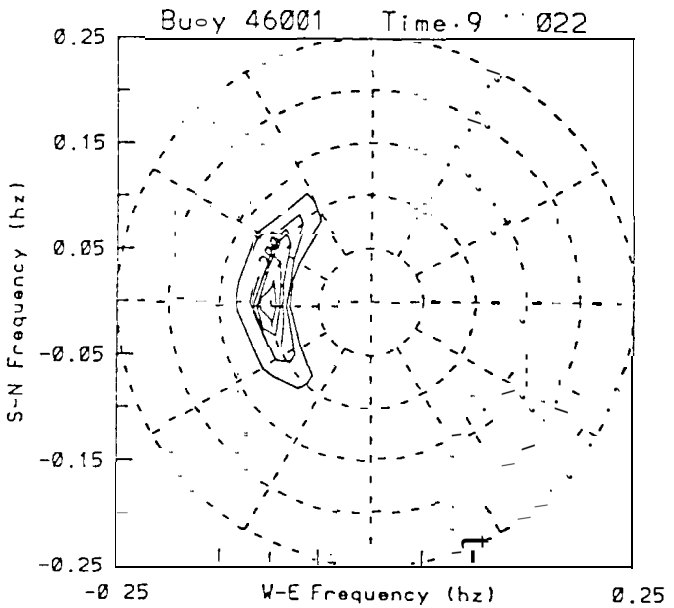

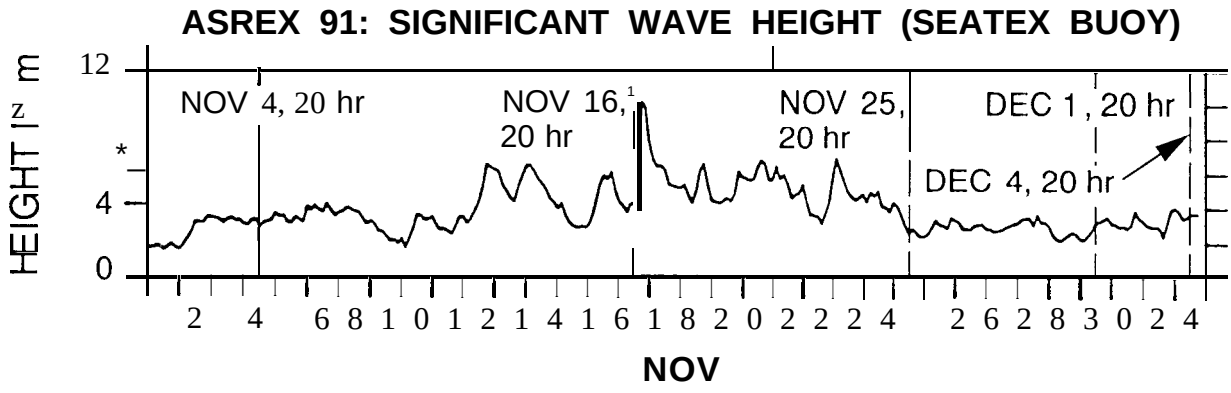
ASREX 91: SIGNIFICANT WAVE HEIGHT (SEATEX BUOY)
HEIGHT IN m
12
4
0
NOV 4, 20 hr
NOV 16, 20 hr
NOV 25, 20 hr
DEC 1, 20 hr
DEC 4, 20 hr
2 4 6 8 10 12 14 16 18 20 22 24 26 28 30 24
NOV

(a)

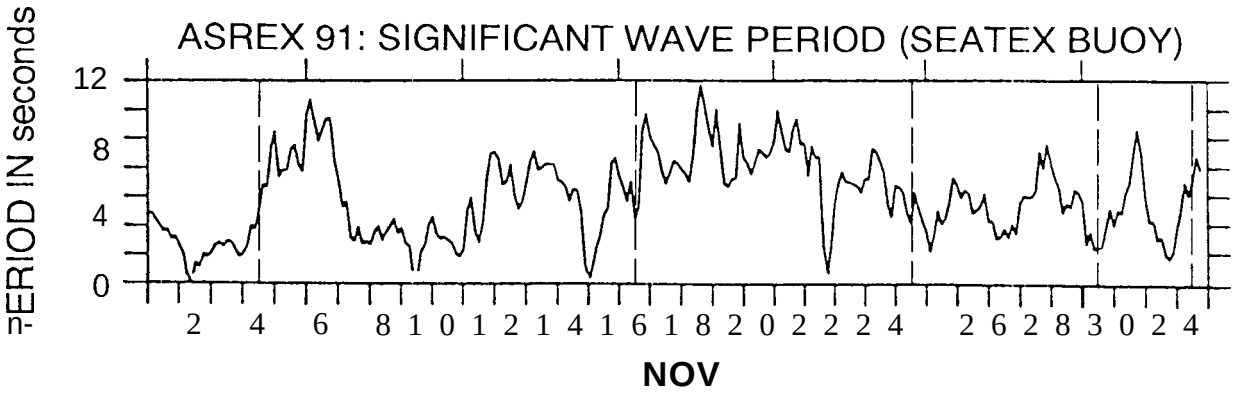
ASREX 91: SIGNIFICANT WAVE PERIOD (SEATEX BUOY)
PERIOD IN seconds
12
8
4
0
2 4 6 8 10 12 14 16 18 20 22 24 26 28 30 24
NOV

(b)

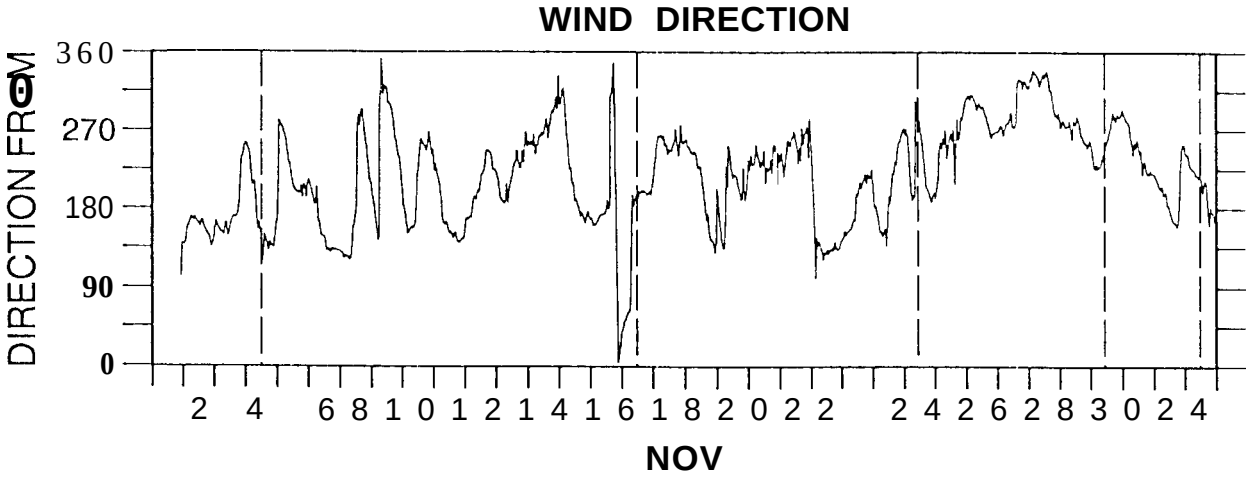
WIND DIRECTION
DIRECTION FROM
360
270
180
90
0
2 4 6 8 10 12 14 16 18 20 22 24 26 28 30 24
NOV

(c)

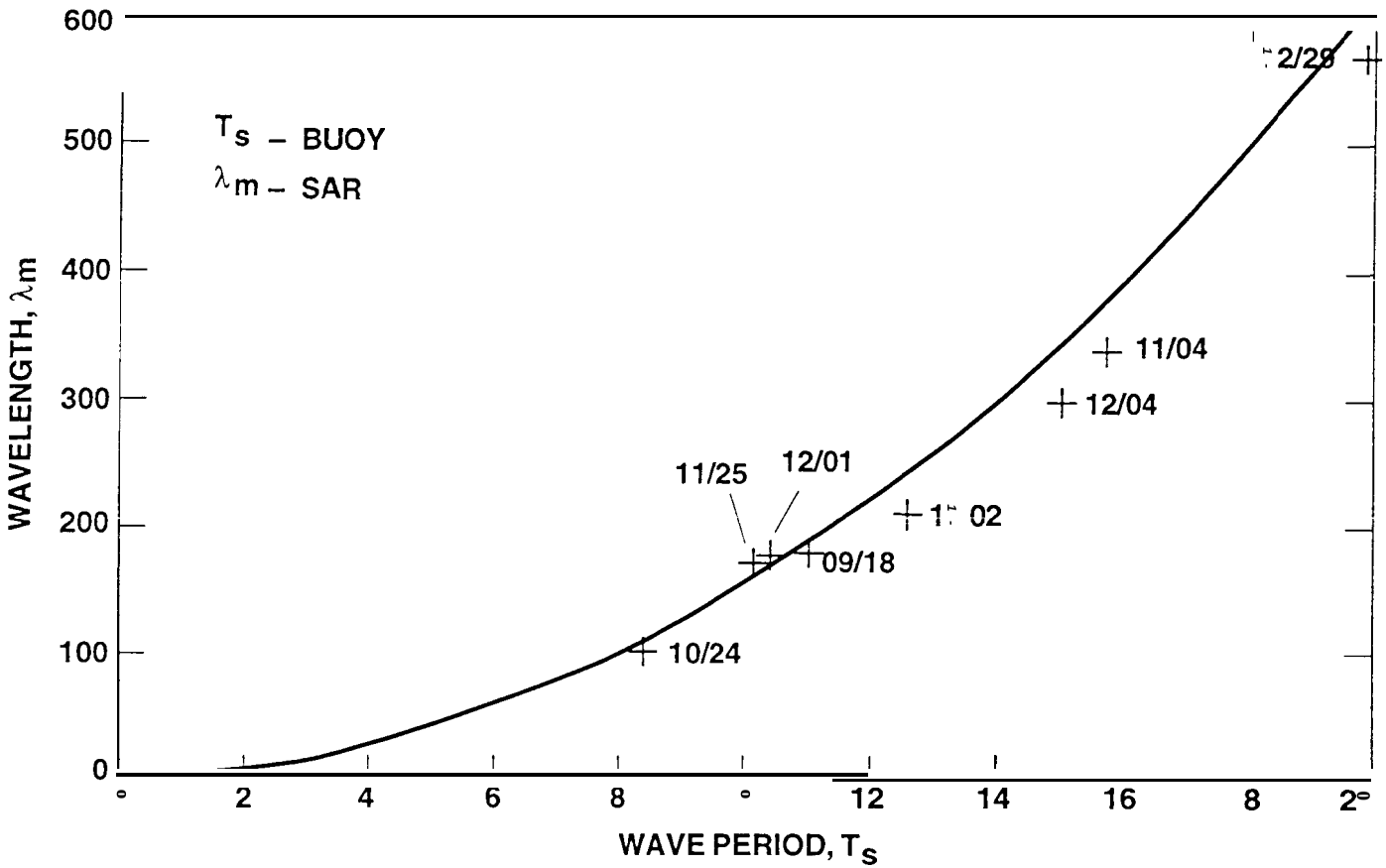
600
500
400
300
200
100
0
WAVELENGTH, λm
Ts – BUOY
λm – SAR
11/25
12/01
09/18
10/24
11/04
12/04
02
2
4
6
8
12
14
16
8
WAVE PERIOD, Ts

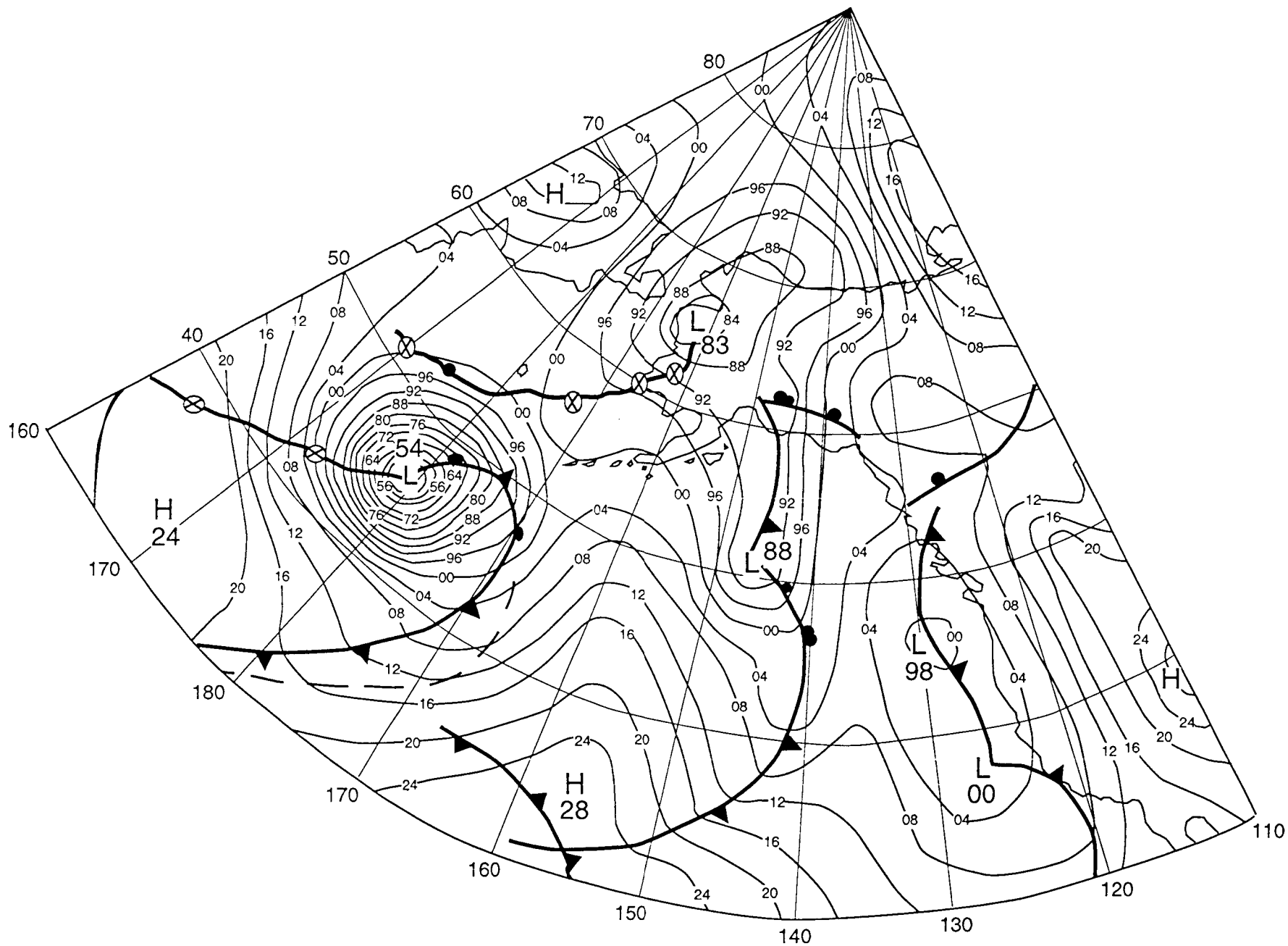
H
24
L
54
L
83
H
H
28
L
88
L
98
L
00
H
80
70
60
50
40
160
170
180
170
160
150
140
130
120
110

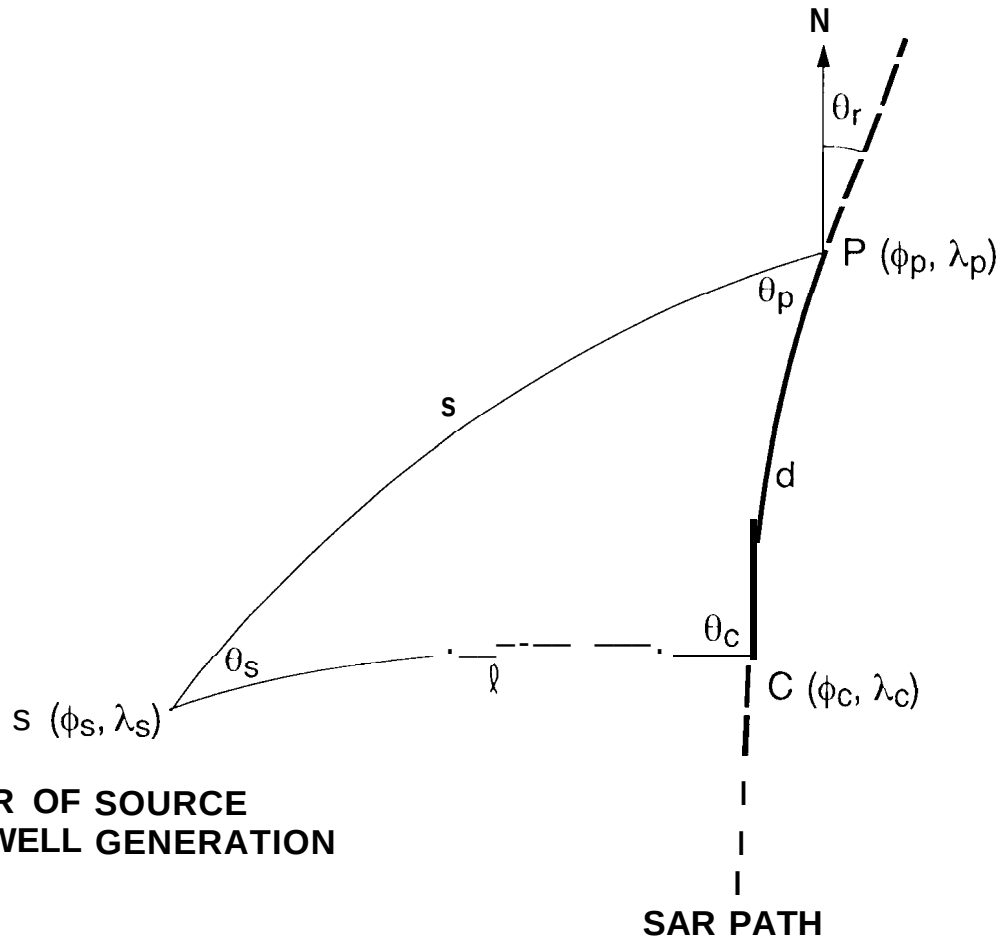
N
θ_r
P (ϕ_p, λ_p)
θ_p
s
d
θ_c
θ_s
ℓ
C (ϕ_c, λ_c)
S (ϕ_s, λ_s)
CENTER OF SOURCE
FOR SWELL GENERATION
SAR PATH

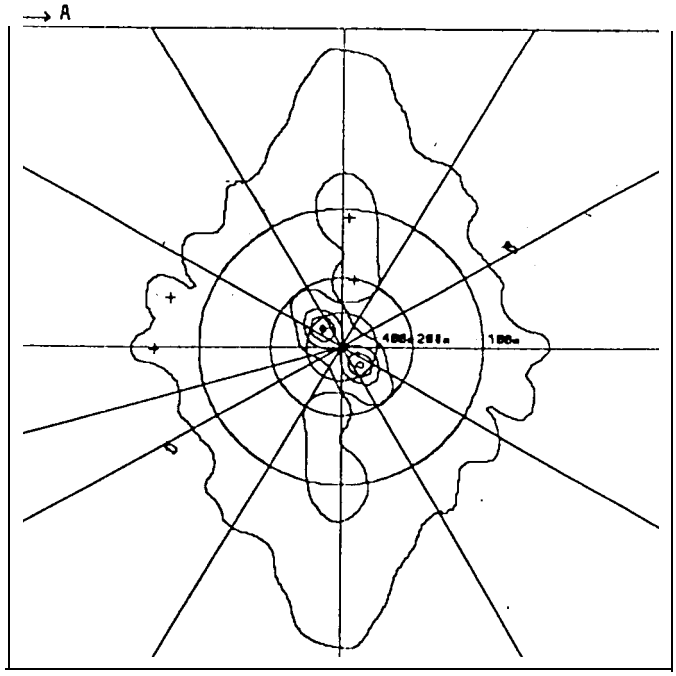

PEAK	WAVE LEN (m)	DIR (deg wrt/N)	PEAK	WAVE LEN (m)	DIR (deg wrt/N)
1	565.7	61.8. 241.8	4	02.9	32.6. 212.6
2	110.2	109.0. 289.0	5	79.0	15.3. 195.3
3	210.4	115.5. 295.5	6	74.9	163.5. 343.5

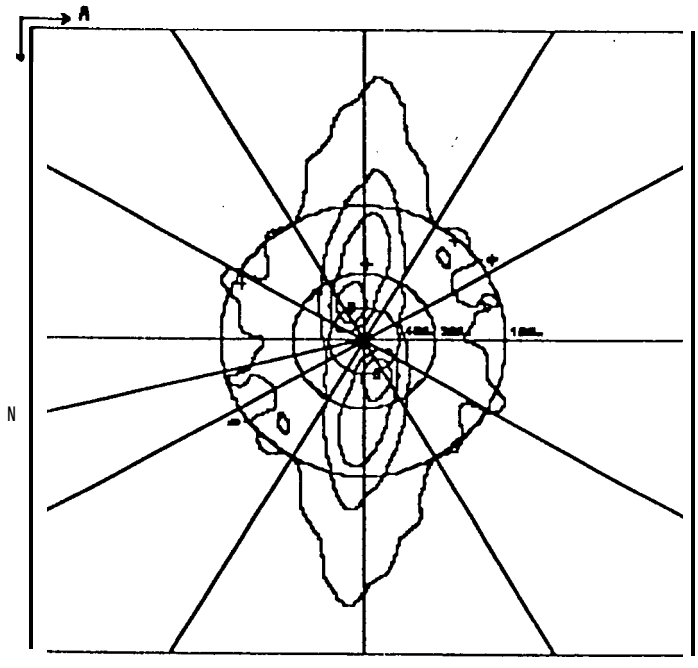

PEAK	WAVE LEN (m)	DIR (deg wrt/N)	PEAK	WAVE LEN (m)	DIR (deg wrt/N)
1	370.2	81.7. 261.7	4	120.1	144.5. 324.5
2	182.8	185.3. 285.3	5	115.8	175.9. 355.9
3	168.4	39.2. 219.2	6	95.4	168.2. 348.2

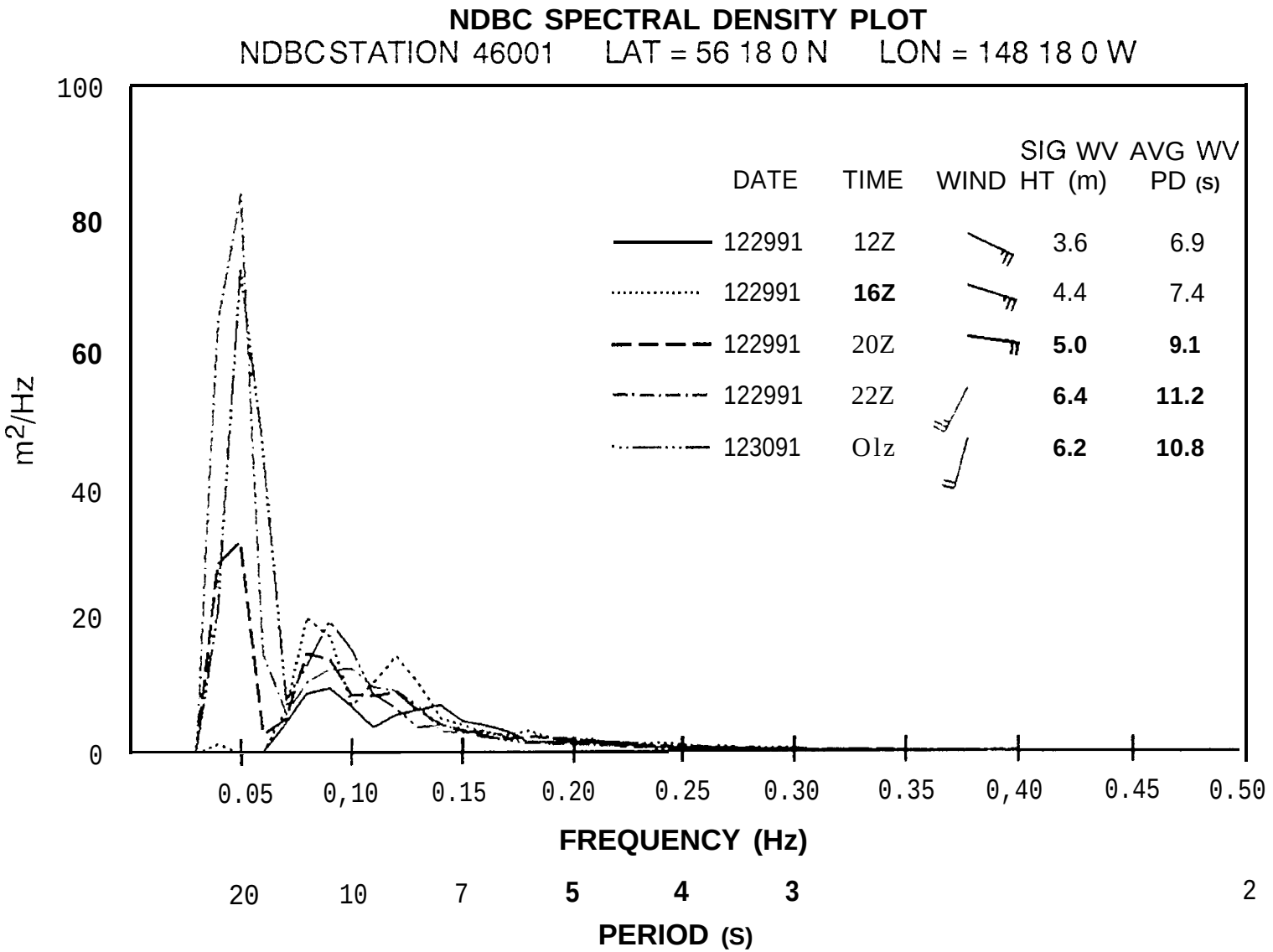
NDBC SPECTRAL DENSITY PLOT
NDBC STATION 46001 LAT = 56 18 0 N LON = 148 18 0 W
DATE TIME WIND SIG WV HT (m) AVG WV PD (s)
122991 12Z 3.6 6.9
122991 16Z 4.4 7.4
122991 20Z 5.0 9.1
122991 22Z 6.4 11.2
123091 Olz 6.2 10.8
m2/Hz
100
80
60
40
20
0
0.05 0,10 0.15 0.20 0.25 0.30 0.35 0,40 0.45 0.50
FREQUENCY (Hz)
20 10 7 5 4 3 2
PERIOD (S)

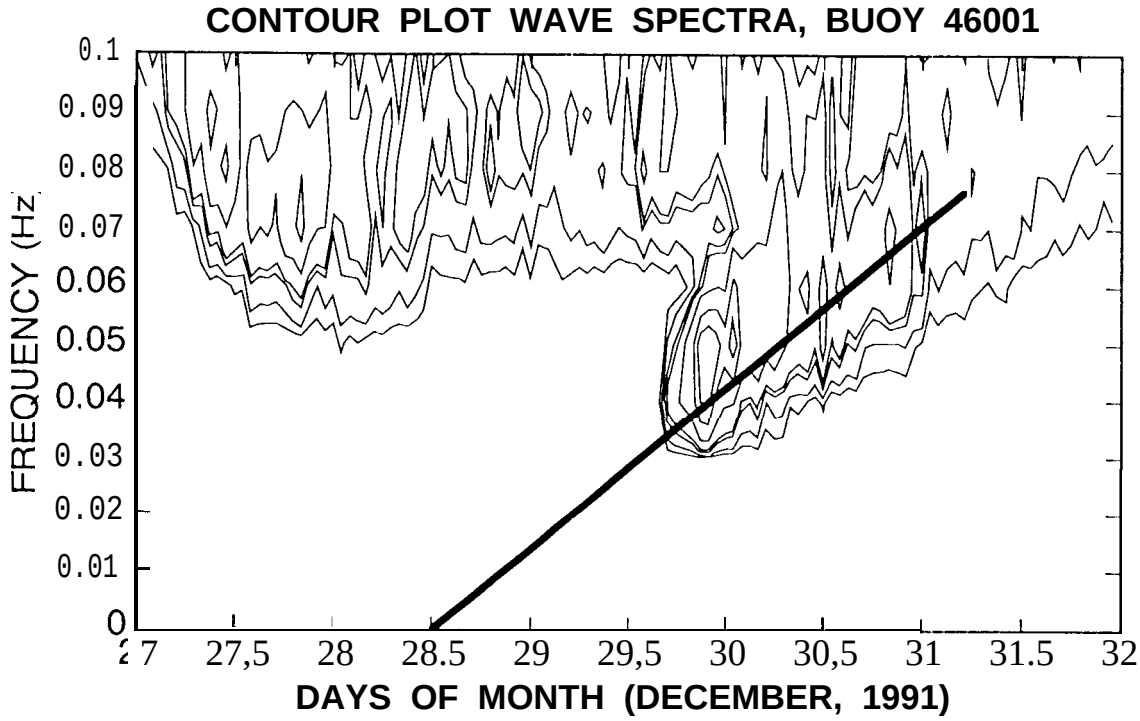
CONTOUR PLOT WAVE SPECTRA, BUOY 46001
FREQUENCY (Hz)
0.1
0.09
0.08
0.07
0.06
0.05
0.04
0.03
0.02
0.01
0
27
27,5
28
28.5
29
29,5
30
30,5
31
31.5
32
DAYS OF MONTH (DECEMBER, 1991)

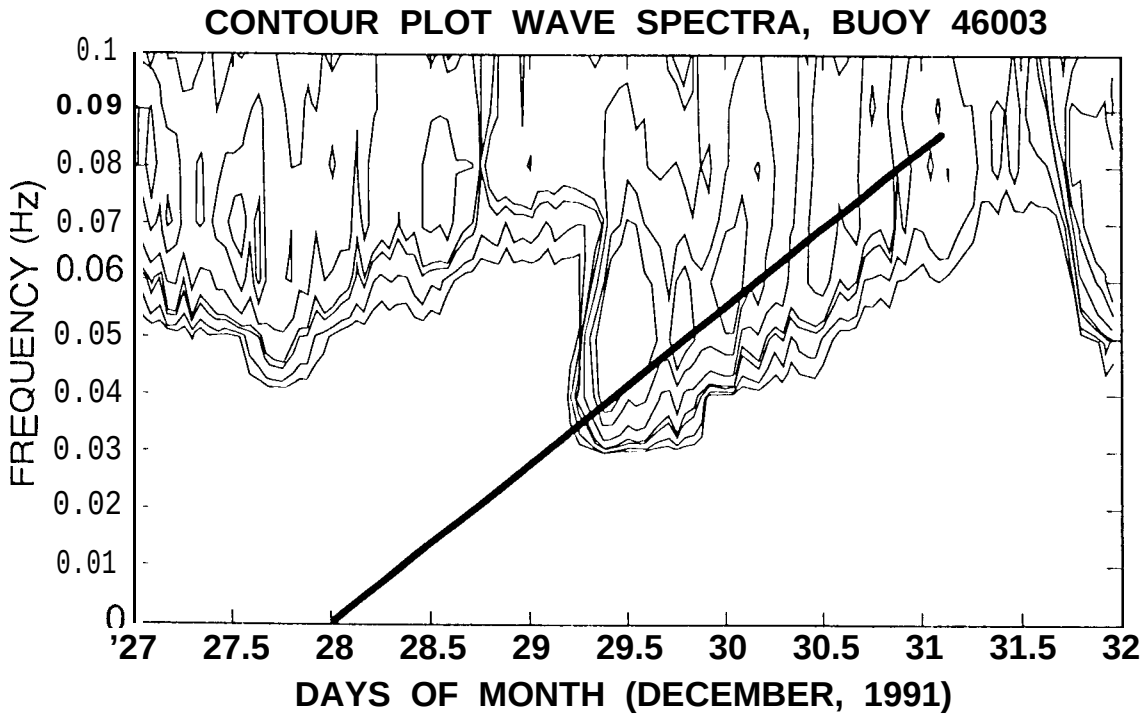
CONTOUR PLOT WAVE SPECTRA, BUOY 46003
FREQUENCY (Hz)
0.1
0.09
0.08
0.07
0.06
0.05
0.04
0.03
0.02
0.01
0
'27
27.5
28
28.5
29
29.5
30
30.5
31
31.5
32
DAYS OF MONTH (DECEMBER, 1991)

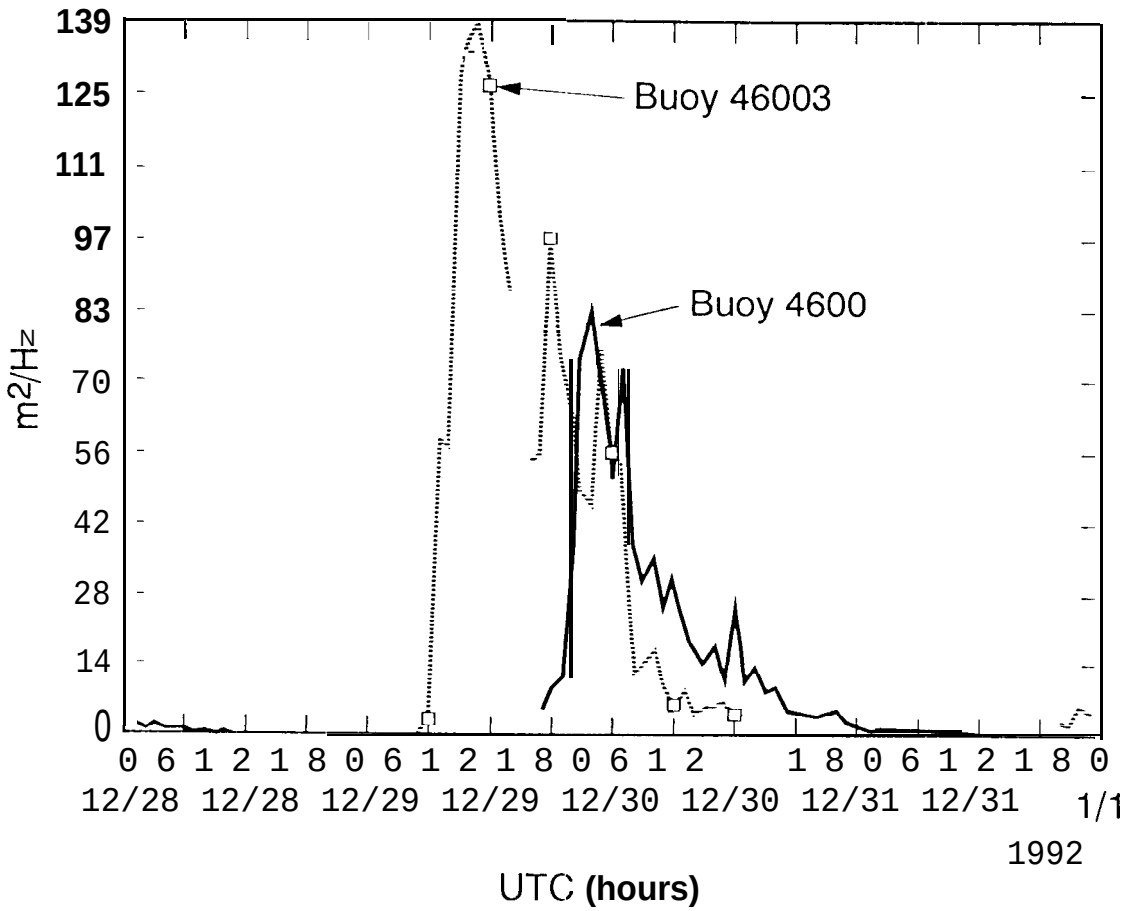
139
125
111
97
83
70
56
42
28
14
0
m2/Hz
Buoy 46003
Buoy 4600
0 6 1 2 1 8 0 6 1 2 1 8 0 6 1 2 1 8 0 6 1 2 1 8 0
12/28 12/28 12/29 12/29 12/30 12/30 12/31 12/31 1/1
1992
UTC (hours)

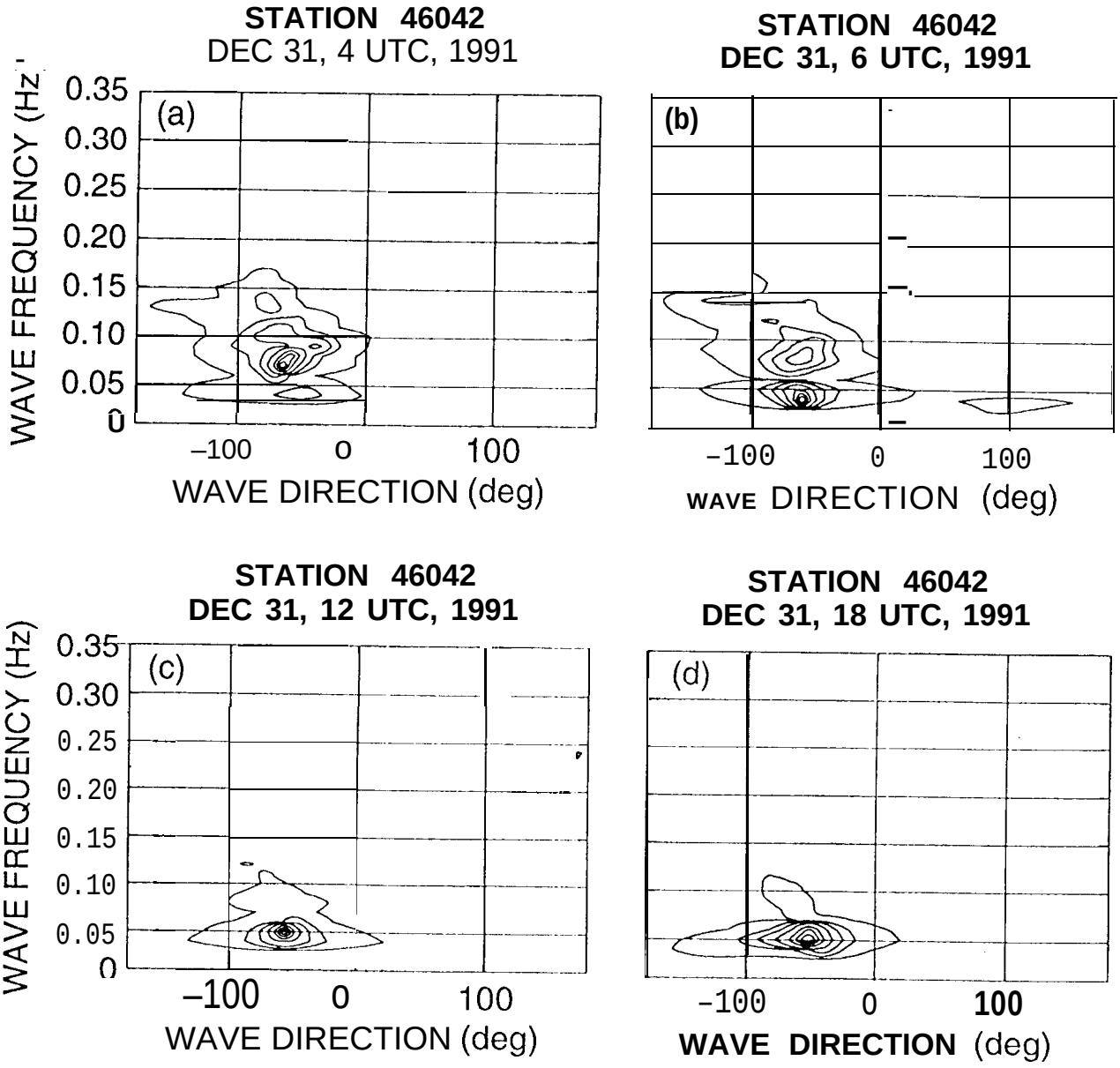
STATION 46042
DEC 31, 4 UTC, 1991
(a)
WAVE FREQUENCY (Hz)
0.35
0.30
0.25
0.20
0.15
0.10
0.05
0
–100
0
100
WAVE DIRECTION (deg)
STATION 46042
DEC 31, 6 UTC, 1991
(b)
–100
0
100
WAVE DIRECTION (deg)
STATION 46042
DEC 31, 12 UTC, 1991
(c)
WAVE FREQUENCY (Hz)
0.35
0.30
0.25
0.20
0.15
0.10
0.05
0
–100
0
100
WAVE DIRECTION (deg)
STATION 46042
DEC 31, 18 UTC, 1991
(d)
–100
0
100
WAVE DIRECTION (deg)